

Origin of the high-energy charge excitations observed by resonant inelastic x-ray scattering in cuprate superconductors

Andrés Greco[†], Hiroyuki Yamase^{*‡}, and Matías Bejas[†]

[†]*Facultad de Ciencias Exactas, Ingeniería y Agrimensura
and Instituto de Física Rosario (UNR-CONICET),
Av. Pellegrini 250, 2000 Rosario, Argentina*

[‡]*National Institute for Materials Science, Tsukuba 305-0047, Japan*

(Dated: February 20, 2022)

Abstract

The recent development of x-ray scattering techniques revealed the charge-excitation spectrum in high- T_c cuprate superconductors. While the presence of a dispersive signal in the high-energy charge-excitation spectrum is well accepted in the electron-doped cuprates, its interpretation and universality are controversial. Since charge fluctuations are observed ubiquitously in cuprate superconductors, the understanding of its origin is a pivotal issue. Here, we employ the layered t - J model with the long-range Coulomb interaction and show that an acoustic-like plasmon mode with a gap at in-plane momentum (0,0) captures the major features of the high-energy charge excitations. The high-energy charge excitations, therefore, should be a universal feature in cuprate superconductors and are expected also in the hole-doped cuprates. Acoustic-like plasmons in cuprates have not been recognized yet in experiments. We propose several experimental tests to distinguish different interpretations of the high-energy charge excitations.

Correspondence to: yamase.hiroyuki@nims.go.jp

Recent progress of x-ray scattering techniques revealed a short-range charge order in hole-doped cuprates (h-cuprates)^{1–11} as well as in electron-doped cuprates (e-cuprates)^{12–14}. To investigate the energy-resolved charge-excitation spectrum, resonant inelastic x-ray scattering (RIXS) is the most powerful tool^{15–17}. RIXS measurements were performed to explore the high-energy region in both e-cuprates^{18–20} and h-cuprates^{21,22}. For e-cuprates, Ref. 18 uncovered that the high-energy charge excitations form a steep dispersion around $\mathbf{q}_{\parallel} = (0, 0)$, where \mathbf{q}_{\parallel} is the in-plane momentum, with an excitation gap about 300 meV at $\mathbf{q}_{\parallel} = (0, 0)$. On the other hand, Refs. 19 and 20 measured charge excitations in a wider \mathbf{q}_{\parallel} region than Ref. 18. The spectrum was found to be typically broad and to become broader toward the Brillouin zone (BZ) boundary. In contrast to Ref. 18, a gap feature around $\mathbf{q}_{\parallel} = (0, 0)$ was not resolved. The observed charge excitations were thus interpreted differently: they may be related to a certain mode near a quantum critical point associated with a symmetry-broken state in Ref. 18, whereas they can be intraband particle-hole excitations with strong incoherent character in Refs. 19 and 20. The situation in h-cuprates is more controversial. Ref. 21 showed that high-energy charge excitations similar to the ones in e-cuprates occur also in h-cuprates, while Ref. 22 emphasized that the high-energy charge excitations are a unique feature in e-cuprates and do not occur in h-cuprates.

Recently, a theoretical study of the layered t - J model with the long-range Coulomb interaction implied that the charge excitation spectrum of cuprates is characterized by a dual structure in the energy space²³. The low-energy charge excitations correspond to various types of bond-charge fluctuations driven by the exchange term (J -term), whereas the high-energy charge excitations are essentially independent of the J -term and come from usual on-site charge fluctuations. In this scenario, the high-energy spectrum is dominated by plasmonic excitations with a finite out-of-plane momentum q_z . The plasmon mode has a gap at $\mathbf{q}_{\parallel} = (0, 0)$ and its magnitude is proportional to the interlayer hopping t_z (Ref. 24). This theoretical proposal provides a third idea to understand the high-energy charge excitations.

Therefore three different ideas are proposed for the origin of the high-energy charge excitations: i) a certain collective mode near a quantum critical point associated with a symmetry-broken state, which should be specific to e-cuprates^{18,22}, ii) intraband particle-hole excitations (not plasmons) present in both e- and h-cuprates^{19–21}, and iii) a plasmon mode with a finite q_z (Ref. 24). In this paper, we show that the plasmon scenario yields results consistent with the experimental observations. We propose several experimental tests

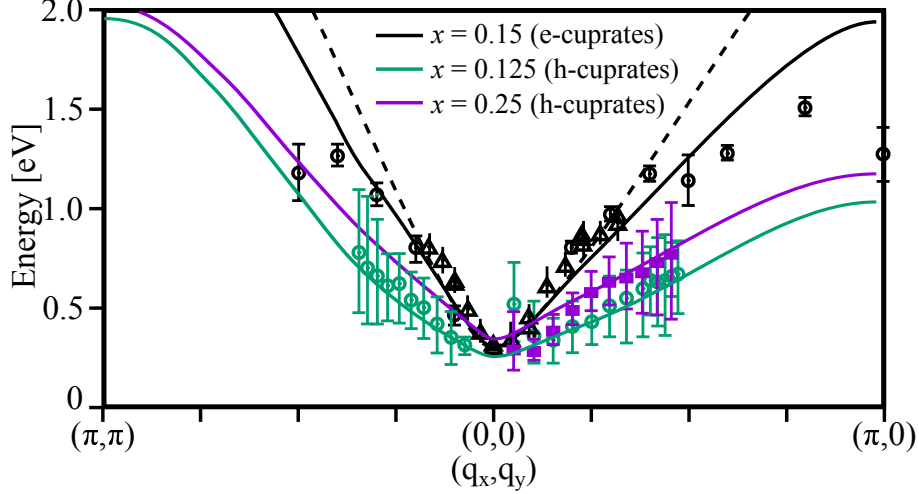


FIG. 1. **Plasmon dispersion.** Our theoretical results are denoted by the black line for e-cuprates with $x = 0.15$, and green and purple lines for h-cuprates with $x = 0.125$ and $x = 0.25$, respectively, along the (π, π) -($0, 0$)-($0, \pi$) direction. For comparison, experimental data are plotted: Black up-triangles and black circles for $\text{Nd}_{2-x}\text{Ce}_x\text{CuO}_4$ with $x = 0.15$ reported in Ref. 18 and Refs. 19 and 20, respectively, and green circles and purple squares for $\text{La}_{2-x}(\text{Br}, \text{Sr})_x\text{CuO}_4$ with $x = 0.125$ and $x = 0.25$, respectively²¹. The dashed line is the dispersion proposed in Ref. 18.

to distinguish different scenarios.

We compute the imaginary part of the usual charge susceptibility $\text{Im}\chi_c(\mathbf{q}, \omega)$ in the layered t - J model with the long-range Coulomb interaction in a large- N scheme (see Methods and Supplemental Material). We show in Fig. 1 the high-energy collective dispersions, namely the peak positions of $\text{Im}\chi_c(\mathbf{q}, \omega)$, for e-cuprates with doping $x = 0.15$ (black line), and for h-cuprates with $x = 0.125$ (green line) and $x = 0.25$ (purple line). These excitations correspond to plasmons realized in the layered system with a gap at $\mathbf{q}_{\parallel} = (0, 0)$. For comparison, we include in Fig. 1 the peak position of the charge excitations obtained in the experiments¹⁸⁻²¹. The agreement with the experimental data is very good in $|\mathbf{q}_{\parallel}| \lesssim 0.5\pi$ for both e- and h-cuprates.

Our obtained dispersion for $x = 0.25$ has higher energy than that for $x = 0.125$. This feature captures the experimental data shown in Fig. 1. In fact, the analysis in Ref. 21 finds that the energy at $\mathbf{q}_{\parallel} = (0.46\pi, 0)$ increases by a factor of 1.16 when doping is increased from $x = 0.125$ to $x = 0.25$. In the present theory, we obtain a factor of 1.30. Similar results were also obtained in the density-matrix renormalization-group calculations in the

three-band Hubbard model²¹.

For $x = 0.15$ in e-cuprates in the large \mathbf{q}_{\parallel} region, i.e., $(0.5\pi, 0)$ - $(\pi, 0)$, the experimental data deviate downward from the dispersion proposed in Ref. 18 (dashed line in Fig. 1) and tend to be closer to our obtained dispersion. Still, the deviation between the experimental data and our results seems substantial, compared with the agreement in the small \mathbf{q}_{\parallel} region. However, we think that such a deviation could be related to, as we shall discuss later, the broad spectrum observed in the experiments especially in a large \mathbf{q}_{\parallel} region.

In addition to the agreement with the experimental data in Fig. 1, the present theory implies the following: i) The high-energy charge excitations correspond to a plasmon mode with a gap at $\mathbf{q}_{\parallel} = (0, 0)$; the gap is proportional to t_z (Ref. 24). ii) Our high-energy charge excitations are present in both e- and h-cuprates. iii) The dispersion around $\mathbf{q}_{\parallel} = (0, 0)$ has a larger slope in e-cuprates than h-cuprates, consistent with the observation in Ref. 21. iv) The dispersion is rather symmetric between the direction $(0, 0)$ - $(\pi, 0)$ and $(0, 0)$ - (π, π) .

Since the plasmon is a collective mode, it can form a very sharp peak in \mathbf{q}_{\parallel} - ω space as shown in Fig. 2a. On the other hand, the experiments of Refs. 19–21 do not show a peak signal at $\mathbf{q}_{\parallel} = (0, 0)$ and in addition, the spectrum is broad and becomes broader with increasing \mathbf{q}_{\parallel} toward the BZ boundary (Fig. 2d). These features are not seen in Fig. 2a because it was computed in an ideal situation by taking $\Gamma = 0.001t$, i.e., the damping is assumed to be very small (see Methods for the definition of Γ). Considering a realistic situation, we compute the charge-excitation spectrum by employing a large Γ . In principle, Γ would depend on momentum and energy, but we take a constant $\Gamma = 0.7t$ as the simplest case. As shown in Fig. 2c, the spectrum is substantially broadened and becomes broader with increasing \mathbf{q}_{\parallel} . In addition, the spectrum near $\mathbf{q}_{\parallel} = (0, 0)$ becomes poorly resolved. These features are very similar to the experimental results (Fig. 2d). In Fig. 2d, there is strong intensity around $\mathbf{q}_{\parallel} = (0, 0)$ and $\omega = 2$ eV, which comes from the charge transfer excitations between oxygens and coppers, namely interband excitations. This feature is beyond the scope of the analysis of the present one-band model.

The inclusion of a large Γ is actually invoked theoretically when the spectral line shape is compared with experiments²¹. In Ref. 24 a finite Γ was also used to discuss the temperature dependence of spectral weight¹⁸. Physically there should be two different broadenings, intrinsic and extrinsic ones. The extrinsic broadening is due to the instrumental resolution, which is about 250 meV ($\Gamma \sim 0.35t$) in Ref. 19, and 130 meV ($\Gamma \sim 0.2t$) in Ref. 18. Because

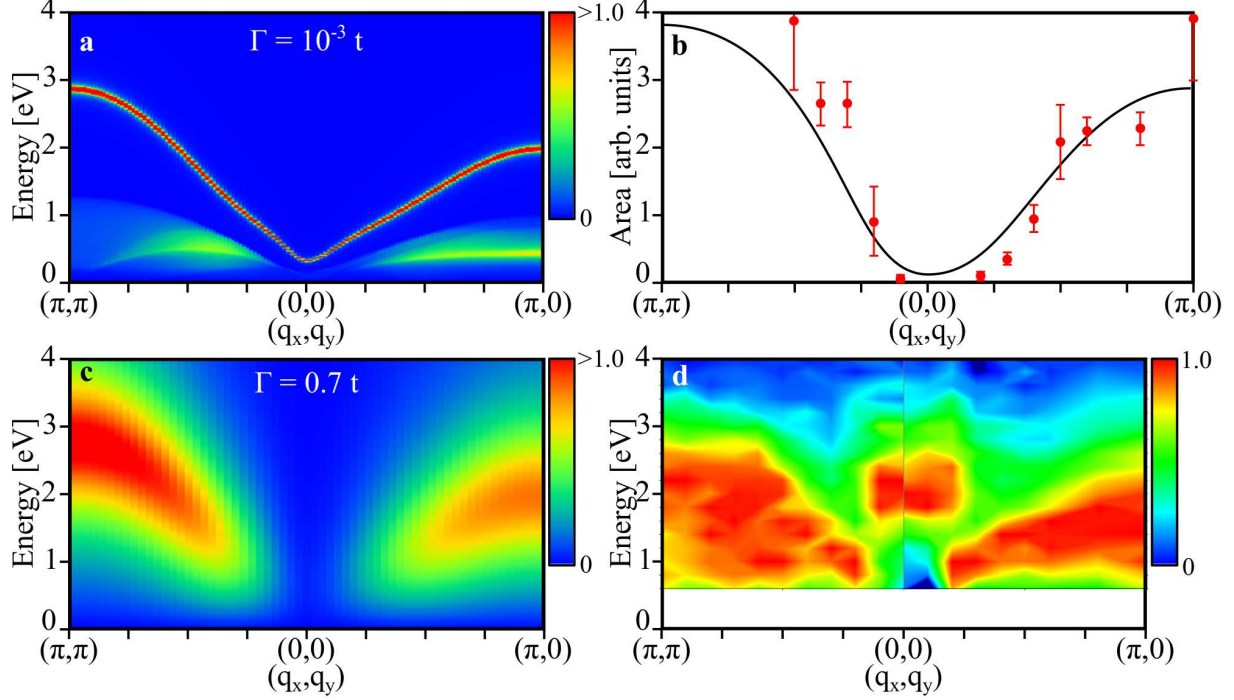


FIG. 2. **Charge excitations for e-cuprates with $x = 0.15$.** **a** and **c**, \mathbf{q}_{\parallel} - ω spectral weight for $\Gamma = 0.001t$ **a** and $\Gamma = 0.7t$ **c**. In **a**, the sharp spectrum (red) comes from plasmons whereas weak intensity around 0.5 eV (green and yellow) is due to individual particle-hole excitations. The experimental result of Fig.2(d) in Ref. 20 is reproduced in **d** for comparison with **c**. **b**, \mathbf{q}_{\parallel} dependence of the peak area obtained from **c**. Red circles are the experimental results for $\text{Nd}_{2-x}\text{Ce}_x\text{CuO}_4$ with $x = 0.15$ (Ref. 20).

of this difference in the instrumental resolution, it is possible that the charge excitation around $\mathbf{q}_{\parallel} = (0,0)$ is resolved in Ref. 18, but not in Ref. 19. In addition, in the low \mathbf{q}_{\parallel} region studied in Ref. 18 the peak width seems to become broader with increasing \mathbf{q}_{\parallel} , consistent with Refs. 19 and 20. The intrinsic broadening comes from incoherent features of high-energy charge excitations due to electron correlation effects as demonstrated in various numerical calculations in the t - J (Refs. 25 and 26) and Hubbard^{19,21} models.

We have also calculated the peak area at a given \mathbf{q}_{\parallel} along the (π, π) -(0,0)-(0, π) direction and compare it with the experimental results in Fig. 2b. This agreement with the experiment strengthens the idea that the high-energy charge excitations are plasmons.

Our plasmon mode should not be confused with usual optical plasmons, which are actually observed in optical measurements²⁷ and electron energy-loss spectroscopy^{28,29} in cuprate

superconductors. The optical plasmon mode is in fact reproduced in our theory by invoking $q_z = 0$ (Ref. 24). However, q_z is usually finite in RIXS. Once q_z becomes finite, the optical plasmon energy is substantially suppressed to be proportional to the interlayer hopping t_z , yielding acoustic-like plasmons as shown in Fig. 1. While this strong q_z dependence was, in part, already discussed in Ref. 24, as well as in early theoretical works where $t_z = 0$ was assumed in a layered model^{30–32}, we present further results. Figure 3 shows a map of the spectral weight of plasmons in the plane of q_z and ω for several choices of Γ at a small \mathbf{q}_{\parallel} . The plasmon energy rapidly decreases with increasing q_z and stays almost constant in $q_z > \pi/3$; this rapid change is more pronounced when a smaller \mathbf{q}_{\parallel} is chosen. The plasmon intensity, on the other hand, increases with increasing q_z , following nearly a q_z^2 dependence at small q_z . Those qualitative features are independent of the broadening Γ . However, the peak intensity at a small \mathbf{q}_{\parallel} is suppressed substantially with increasing Γ (see also Fig. 2c). Hence the q_z dependence of plasmons may be well observed for a small Γ . Although the importance of the q_z dependence of plasmons was not recognized in experimental papers^{18–22}, we have learned that results similar to Fig. 3 are recently obtained in RIXS (Ref. 33).

The reason why plasmons show a strong q_z dependence is easily understood by recalling that plasmons originate from the singularity of the long-range Coulomb interaction in the limit of long wavelength. A special feature of the present layered model lies in the anisotropy of the momentum dependence of the long-range Coulomb interaction $V(\mathbf{q})$ [see Eq. (2)]. When $q_z = 0$, $V(\mathbf{q})$ is singular at $\mathbf{q}_{\parallel} = (0, 0)$, which leads to usual optical plasmons. However, due to the anisotropy between \mathbf{q}_{\parallel} and q_z , the plasmon energy becomes different when q_z is reduced to zero at $\mathbf{q}_{\parallel} = (0, 0)$. In particular, the plasmon energy would become zero if the interlayer hopping is neglected. This is the reason why the plasmon energy becomes sensitive to the value of q_z , especially in a region of a small \mathbf{q}_{\parallel} .

We have shown that acoustic-like plasmon excitations with a gap at $\mathbf{q}_{\parallel} = (0, 0)$ due to a finite interlayer hopping describe the main features observed by different experimental groups^{18–21} in a consistent way. How about other scenarios?

The scenario proposed in Refs. 18 and 22 invokes a collective mode associated with a certain symmetry-broken state to understand the high-energy charge excitations around $\mathbf{q}_{\parallel} = (0, 0)$. The crucial point of this scenario is that their hypothetical order should be specific to e-cuprates, because Refs. 18 and 22 claim that similar charge excitations around $\mathbf{q}_{\parallel} = (0, 0)$ are not present in h-cuprates at least from their RIXS measurements using

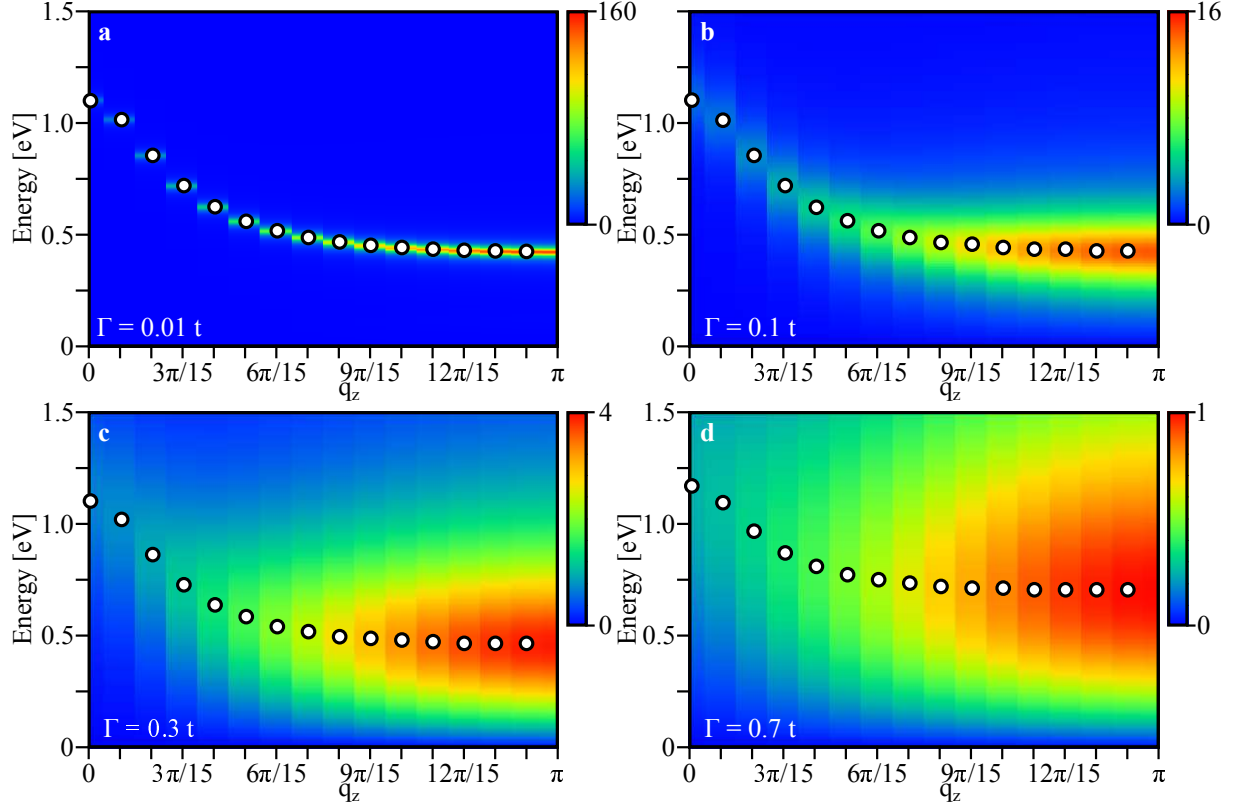


FIG. 3. **Intensity maps of plasmons in the plane of q_z and ω .** The in-plane momentum \mathbf{q}_{\parallel} is set to $(0.05\pi, 0.05\pi)$ and the four panels correspond to different values of the broadening Γ . The open circles denotes the peak position at each q_z .

the Cu L_3 -edge. However, both spin and charge excitations are detected in the Cu L_3 -edge and the intensity from the later can be lower than the former. In fact, recently Ref. 21 successfully detects the high-energy charge excitations also in h-cuprates by using the oxygen K -edge RIXS, which can probe directly the charge dynamics of doped holes. This recent experimental data is not reconciled with the scenario proposed in Refs. 18 and 22. Thus, in order to discriminate the scenario of Refs. 18 and 22 from the others, it is crucial to test the presence of high-energy charge excitations in h-cuprates by different experimental groups.

Refs. 19–21 propose intraband charge excitations and emphasize their incoherent character. This scenario can be interpreted in two different ways. On one hand, our acoustic-like plasmons are also from intraband particle-hole excitations and their experimental data (Figs. 1, 2b, and 2d) are well captured by introducing a large Γ (Figs. 2b and 2c). Therefore their scenario can be understood in terms of plasmons with a large damping, although this possibility was not discussed in Refs. 19–21. On the other hand, incoherent intraband

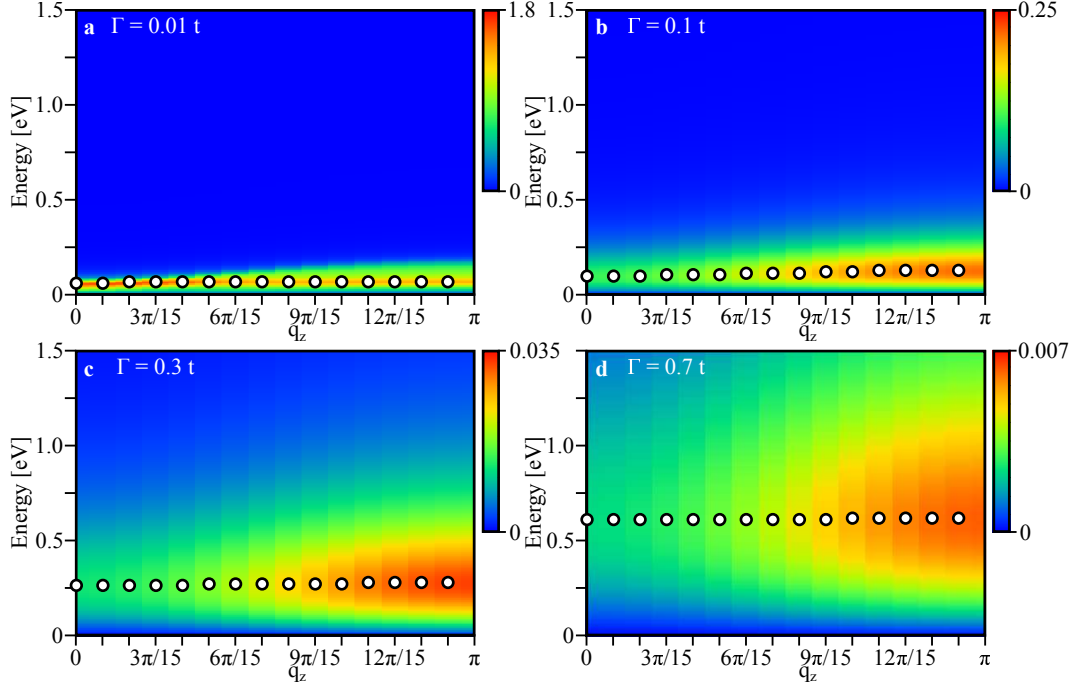


FIG. 4. **Intensity maps of individual particle-hole excitations in the plane of q_z and ω .** The parameters are the same as those in Fig. 3.

excitations occur also as individual charge excitations, which form the continuum spectrum below the plasmon energy. In this case, two predictions are possible. First, charge excitations should be gapless at $\mathbf{q}_{\parallel} = (0, 0)$. Although a region around $\mathbf{q}_{\parallel} = (0, 0)$ was not resolved below 2 eV in their measurements (see Fig. 2d), Ref. 18 reports a gap feature (see also Fig. 1). Therefore, besides Ref. 18, it is decisively important to confirm the presence of a charge gap at $\mathbf{q}_{\parallel} = (0, 0)$ by different experimental groups. The second prediction concerns the q_z dependence of the charge excitations. We have computed the q_z dependence of individual charge excitations in our model as shown in Fig. 4 (see Supplemental Material for details). While the peak position depends on choices of Γ , its q_z dependence is almost negligible. This feature is qualitatively different from plasmons shown in Fig. 3 and thus serves to clarify the underlying physics of the high-energy charge excitations.

One may wish to consider a scenario without the long-range Coulomb interaction, which may replace plasmons with a zero-sound mode in the t - J model. To demonstrate this, we have computed charge excitations in our model by using the short-range Coulomb interaction instead of the long-range one (see Supplemental Material). Our obtained spectrum is shown in Fig. 5a, which is qualitatively similar to Fig. 2a. While it is clear theoretically that the

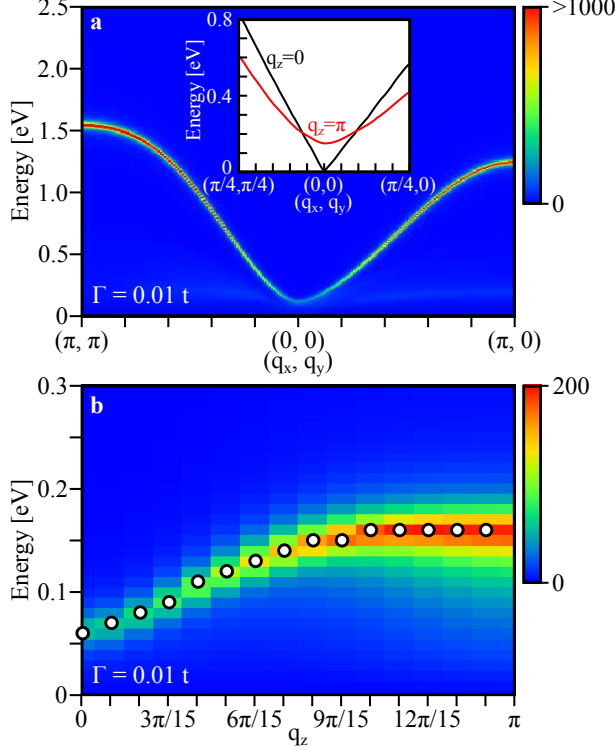


FIG. 5. **Intensity maps of charge excitations without the long-range Coulomb interaction.** **a**, \mathbf{q}_{\parallel} - ω spectral weight for $q_z = \pi$, a similar plot to Fig. 2a; $\Gamma = 0.01t$ is taken for numerical convenience. The sharp spectrum describes a zero-sound mode. **Inset**, zero-sound dispersion for $q_z = \pi$ and 0 around $\mathbf{q}_{\parallel} = (0, 0)$. **b**, q_z dependence of the intensity at $\mathbf{q}_{\parallel} = (0.02\pi, 0.02\pi)$, a similar plot to Fig. 3.

zero-sound mode is fundamentally different from plasmons³⁴, their distinction is less clear from an experimental point of view. Hence, we have computed the q_z dependence of the zero-sound mode for a small \mathbf{q}_{\parallel} in Fig. 5b. The zero-sound energy *increases* with increasing q_z in a small q_z region, which is qualitatively different from the plasmon case shown in Fig. 3. This is because the zero-sound mode becomes gapless at $\mathbf{q}_{\parallel} = (0, 0)$ and $q_z = 0$ as shown in the inset of Fig. 5a. Therefore, besides Ref. 33, additional experimental data about the q_z dependence of the high-energy charge excitations may confirm the importance of the long-range Coulomb interaction in the charge dynamics in cuprates.

We have demonstrated that acoustic-like plasmon excitations can consistently explain experimental data obtained by different groups^{18–21}. Conceptually plasmons are well known in solids, but the presence of the acoustic-like plasmon mode in cuprates has not been recog-

nized yet in experiments. Thus our theoretical recognition of the acoustic-like plasmons in cuprates highlights the importance of charge dynamics in cuprates. Recalling that cuprates have been studied largely by focusing on spin degrees of freedom, it is worth exploring unresolved issues in cuprates such as the origin of the pseudogap and the mechanism of high- T_c superconductivity in terms of charge degrees of freedom, including the present acoustic-like plasmons.

Methods

We employ the t - J model on a square lattice by including the interlayer hopping and the long-range Coulomb interaction:

$$H = - \sum_{i,j,\sigma} t_{ij} \tilde{c}_{i\sigma}^\dagger \tilde{c}_{j\sigma} + \sum_{\langle i,j \rangle} J_{ij} \left(\vec{S}_i \cdot \vec{S}_j - \frac{1}{4} n_i n_j \right) + \frac{1}{2} \sum_{i,j} V_{ij} n_i n_j \quad (1)$$

where $\tilde{c}_{i\sigma}^\dagger$ and $\tilde{c}_{i\sigma}$ are the creation and annihilation operators of electrons with spin σ in the Fock space without double occupancy, and i and j run over a three-dimensional lattice. $n_i = \sum_{\sigma} \tilde{c}_{i\sigma}^\dagger \tilde{c}_{i\sigma}$ is the electron density operator and \vec{S}_i is the spin operator. The hopping t_{ij} takes a value t (t') between the first (second) nearest-neighbors sites on the square lattice, and t_z between the layers. $\langle i, j \rangle$ denotes a nearest-neighbor pair of sites. We neglect the magnetic exchange interaction between the planes, which is much smaller than in-plane J (Ref. 35). V_{ij} is the long-range Coulomb interaction on the lattice and it is given in momentum space by³⁶

$$V(\mathbf{q}) = \frac{V_c}{A(q_x, q_y) - \cos q_z}, \quad (2)$$

where $V_c = e^2 d (2\epsilon_\perp a^2)^{-1}$ and

$$A(q_x, q_y) = \alpha(2 - \cos q_x - \cos q_y) + 1, \quad (3)$$

where $\alpha = (d/a)^2 \epsilon_\parallel / \epsilon_\perp$, and ϵ_\parallel and ϵ_\perp are the dielectric constants parallel and perpendicular to the planes, respectively; e is the electric charge of electrons; a is the lattice constant in the planes and the in-plane momentum $\mathbf{q}_\parallel = (q_x, q_y)$ is measured in units of a^{-1} ; similarly d is the distance between the planes and the out-of-plane momentum q_z is measured in units of d^{-1} .

Since the Hamiltonian (1) is defined in the Fock space without double occupancy, its analysis is not straightforward. Here we use a large- N technique based on path integral

representation of the Hubbard X operators^{37,38}, which was extended to a layered model in Ref. 24. In Supplemental Material, we present the essential part of our formalism.

The model Hamiltonian (1) contains several parameters, which may depend on materials. Fixing a value of J and the long-range Coulomb interaction $V(\mathbf{q})$ as $J/t = 0.3$ (Ref. 39), and $V_c/t = 17$ and $\alpha = 4.5$ (Ref. 24), respectively, we allow a material dependence of the other parameters: $t'/t = 0.30$ and $t_z/t = 0.1$ for $\text{Nd}_{2-x}\text{Ce}_x\text{CuO}_4$ (Ref. 24), and $t'/t = -0.20$ and $t_z/t = 0.05$ (Ref. 40) for $\text{La}_{2-x}(\text{Br},\text{Sr})_x\text{CuO}_4$. It would also be possible to assume a similar value of t_z between them and to take a slightly different values of V_c and α . However, we do not attempt such a tuning. Instead we aim to capture the major features of charge-excitation spectrum with a minimal change of the parameters. We take the number of layers as $N_z = 30$, which should be large enough. To address the high-energy charge-excitation spectrum, we compute the imaginary part of the usual charge susceptibility $\chi_c(\mathbf{q}, i\omega_n)$ after analytical continuation $i\omega_n \rightarrow \omega + i\Gamma$ in Eq. (S9) in Supplemental Material, where Γ is positive and, in principle, infinitesimally small. In RIXS, the interlayer momentum transfer q_z is usually finite. We thus first present results for $q_z = \pi$ as representative ones in Figs. 1 and 2, and then study their q_z dependence. The temperature is set to zero.

In the comparison with the experimental data in Fig. 1, we have used $t = 750$ meV for $\text{Nd}_{2-x}\text{Ce}_x\text{CuO}_4$ and $t = 500$ meV for $\text{La}_{2-x}(\text{Br},\text{Sr})_x\text{CuO}_4$. The value of t for the former is somewhat larger than the accepted value³⁹. A possible reason lies in the renormalization of the bare hopping t in the large- N scheme, i.e., $t \rightarrow t\frac{x}{2}$ [see Eqs. (S7) and (S8) in Supplemental Material], which is simply reduced by x and thus can be simple quantitatively.

Author contributions

A. G. and H. Y. contributed equally to the present project and managed it together. H. Y. wrote the major part of the manuscript, and A. G. and M. B. performed numerical calculations of the charge susceptibility.

Acknowledgments

The authors thank T. Devereaux, K. Ishii, and T. Tohyama for very fruitful discussions, and K. Ishii for providing them the experimental data in Fig. 2b. H. Y. acknowledges support by JSPS KAKENHI Grant Number JP15K05189. A. G. acknowledges the Japan Society for the Promotion of Science for a Short-term Invitational Fellowship program (S17027), under

which this work was initiated.

-
- ¹ Ghiringhelli, G. *et al.* Long-Range Incommensurate Charge Fluctuations in (Y,Nd)Ba₂Cu₃O_{6+x}. *Science* **337**, 821–825 (2012). URL <http://science.sciencemag.org/content/337/6096/821>.
- ² Chang, J. *et al.* Direct observation of competition between superconductivity and charge density wave order in YBa₂Cu₃O_{6.67}. *Nature Physics* **8**, 871 (2012). URL <http://dx.doi.org/10.1038/nphys2456>.
- ³ Achkar, A. J. *et al.* Distinct Charge Orders in the Planes and Chains of Ortho-III-Ordered YBa₂Cu₃O_{6+δ} Superconductors Identified by Resonant Elastic X-ray Scattering. *Phys. Rev. Lett.* **109**, 167001 (2012). URL <https://link.aps.org/doi/10.1103/PhysRevLett.109.167001>.
- ⁴ Blackburn, E. *et al.* X-Ray Diffraction Observations of a Charge-Density-Wave Order in Superconducting Ortho-II YBa₂Cu₃O_{6.54} Single Crystals in Zero Magnetic Field. *Phys. Rev. Lett.* **110**, 137004 (2013). URL <https://link.aps.org/doi/10.1103/PhysRevLett.110.137004>.
- ⁵ Blanco-Canosa, S. *et al.* Resonant x-ray scattering study of charge-density wave correlations in YBa₂Cu₃O_{6+x}. *Phys. Rev. B* **90**, 054513 (2014). URL <https://link.aps.org/doi/10.1103/PhysRevB.90.054513>.
- ⁶ Comin, R. *et al.* Charge Order Driven by Fermi-Arc Instability in Bi₂Sr_{2-x}La_xCuO_{6+δ}. *Science* **343**, 390–392 (2014). URL <http://science.sciencemag.org/content/343/6169/390>.
- ⁷ da Silva Neto, E. H. *et al.* Ubiquitous interplay between charge ordering and high-temperature superconductivity in cuprates. *Science* **343**, 393–396 (2014). URL <http://science.sciencemag.org/content/343/6169/393>.
- ⁸ Tabis, W. *et al.* Charge order and its connection with Fermi-liquid charge transport in a pristine high-*T_c* cuprate. *Nature Communications* **5**, 5875 (2014). URL <http://dx.doi.org/10.1038/ncomms6875>.
- ⁹ Gerber, S. *et al.* Three-dimensional charge density wave order in YBa₂Cu₃O_{6.67} at high magnetic fields. *Science* **350**, 949–952 (2015). URL <http://science.sciencemag.org/content/350/6263/949>.
- ¹⁰ Chang, J. *et al.* Magnetic field controlled charge density wave coupling in underdoped YBa₂Cu₃O_{6+x}. *Nature Communications* **7**, 11494 (2016). URL <http://dx.doi.org/10.1038/ncomms11494>.

- ¹¹ Tabis, W. *et al.* Synchrotron x-ray scattering study of charge-density-wave order in $\text{HgBa}_2\text{CuO}_{4+\delta}$. *Phys. Rev. B* **96**, 134510 (2017). URL <https://link.aps.org/doi/10.1103/PhysRevB.96.134510>.
- ¹² da Silva Neto, E. H. *et al.* Charge ordering in the electron-doped superconductor $\text{Nd}_{2-x}\text{Ce}_x\text{CuO}_4$. *Science* **347**, 282–285 (2015). URL <http://science.sciencemag.org/content/347/6219/282>.
- ¹³ da Silva Neto, E. H. *et al.* Doping-dependent charge order correlations in electron-doped cuprates. *Science Advances* **2**, e1600782 (2016). URL <http://advances.sciencemag.org/content/2/8/e1600782>.
- ¹⁴ da Silva Neto, E. H. *et al.* Coupling between dynamic magnetic and charge-order correlations in the cuprate superconductor $\text{Nd}_{2-x}\text{Ce}_x\text{CuO}_4$. *ArXiv e-prints* (2018). 1804.09185.
- ¹⁵ Hashimoto, M. *et al.* Direct observation of bulk charge modulations in optimally doped $\text{Bi}_{1.5}\text{Pb}_{0.6}\text{Sr}_{1.54}\text{CaCu}_2\text{O}_{8+\delta}$. *Phys. Rev. B* **89**, 220511 (2014). URL <https://link.aps.org/doi/10.1103/PhysRevB.89.220511>.
- ¹⁶ Peng, Y. Y. *et al.* Direct observation of charge order in underdoped and optimally doped $\text{Bi}_2(\text{Sr},\text{La})_2\text{CuO}_{6+\delta}$ by resonant inelastic x-ray scattering. *Phys. Rev. B* **94**, 184511 (2016). URL <https://link.aps.org/doi/10.1103/PhysRevB.94.184511>.
- ¹⁷ Chaix, L. *et al.* Dispersive charge density wave excitations in $\text{Bi}_2\text{Sr}_2\text{CaCu}_2\text{O}_{8+\delta}$. *Nature Physics* **13**, 952 (2017). URL <http://dx.doi.org/10.1038/nphys4157>.
- ¹⁸ Lee, W. S. *et al.* Asymmetry of collective excitations in electron- and hole-doped cuprate superconductors. *Nature Physics* **10**, 883 (2014). URL <http://dx.doi.org/10.1038/nphys3117>.
- ¹⁹ Ishii, K. *et al.* High-energy spin and charge excitations in electron-doped copper oxide superconductors. *Nature Communications* **5**, 3714 (2014). URL <http://dx.doi.org/10.1038/ncomms4714>.
- ²⁰ Ishii, K. *et al.* Momentum Dependence of Charge Excitations in the Electron-Doped Superconductor $\text{Nd}_{1.85}\text{Ce}_{0.15}\text{CuO}_4$: A Resonant Inelastic X-Ray Scattering Study. *Phys. Rev. Lett.* **94**, 207003 (2005). URL <https://link.aps.org/doi/10.1103/PhysRevLett.94.207003>.
- ²¹ Ishii, K. *et al.* Observation of momentum-dependent charge excitations in hole-doped cuprates using resonant inelastic x-ray scattering at the oxygen K edge. *Phys. Rev. B* **96**, 115148 (2017). URL <https://link.aps.org/doi/10.1103/PhysRevB.96.115148>.
- ²² Dellea, G. *et al.* Spin and charge excitations in artificial hole- and electron-doped

- infinite layer cuprate superconductors. *Phys. Rev. B* **96**, 115117 (2017). URL <https://link.aps.org/doi/10.1103/PhysRevB.96.115117>.
- ²³ Bejas, M., Yamase, H. & Greco, A. Dual structure in the charge excitation spectrum of electron-doped cuprates. *Phys. Rev. B* **96**, 214513 (2017). URL <https://link.aps.org/doi/10.1103/PhysRevB.96.214513>.
- ²⁴ Greco, A., Yamase, H. & Bejas, M. Plasmon excitations in layered high- T_c cuprates. *Phys. Rev. B* **94**, 075139 (2016). URL <https://link.aps.org/doi/10.1103/PhysRevB.94.075139>.
- ²⁵ Prelovšek, P. & Horsch, P. Electron-energy loss spectra and plasmon resonance in cuprates. *Phys. Rev. B* **60**, R3735–R3738 (1999). URL <https://link.aps.org/doi/10.1103/PhysRevB.60.R3735>.
- ²⁶ Tohyama, T., Horsch, P. & Maekawa, S. Spin and Charge Dynamics of the $t - J$ Model. *Phys. Rev. Lett.* **74**, 980–983 (1995). URL <https://link.aps.org/doi/10.1103/PhysRevLett.74.980>.
- ²⁷ Singley, E. J., Basov, D. N., Kurahashi, K., Uefuji, T. & Yamada, K. Electron dynamics in $\text{Nd}_{1.85}\text{Ce}_{0.15}\text{CuO}_{4+\delta}$: Evidence for the pseudogap state and unconventional c-axis response. *Phys. Rev. B* **64**, 224503 (2001). URL <https://link.aps.org/doi/10.1103/PhysRevB.64.224503>.
- ²⁸ Nücker, N. *et al.* Plasmons and interband transitions in $\text{Bi}_2\text{Sr}_2\text{CaCu}_2\text{O}_8$. *Phys. Rev. B* **39**, 12379–12382 (1989). URL <https://link.aps.org/doi/10.1103/PhysRevB.39.12379>.
- ²⁹ Romberg, H. *et al.* Dielectric function of $\text{YBa}_2\text{Cu}_3\text{O}_{7-\delta}$ between 50 meV and 50 eV. *Zeitschrift für Physik B Condensed Matter* **78**, 367–380 (1990). URL <https://doi.org/10.1007/BF01313317>.
- ³⁰ Kresin, V. Z. & Morawitz, H. Layer plasmons and high- T_c superconductivity. *Phys. Rev. B* **37**, 7854–7857 (1988). URL <https://link.aps.org/doi/10.1103/PhysRevB.37.7854>.
- ³¹ Bill, A., Morawitz, H. & Kresin, V. Z. Electronic collective modes and superconductivity in layered conductors. *Phys. Rev. B* **68**, 144519 (2003). URL <https://link.aps.org/doi/10.1103/PhysRevB.68.144519>.
- ³² Markiewicz, R. S., Hasan, M. Z. & Bansil, A. Acoustic plasmons and doping evolution of mott physics in resonant inelastic x-ray scattering from cuprate superconductors. *Phys. Rev. B* **77**, 094518 (2008). URL <https://link.aps.org/doi/10.1103/PhysRevB.77.094518>.
- ³³ Hepting, M. *et al.* Three-dimensional collective charge excitations in electron-doped copper oxide superconductors. *Nature* (2018). URL <https://doi.org/10.1038/s41586-018-0648-3>.

- ³⁴ Negele, J. W. & Orland, H. *Quantum Many-Particle Systems* (Perseus Books Publishing, 1998).
- ³⁵ Thio, T. *et al.* Antisymmetric exchange and its influence on the magnetic structure and conductivity of La_2CuO_4 . *Phys. Rev. B* **38**, 905–908 (1988). URL <https://link.aps.org/doi/10.1103/PhysRevB.38.905>.
- ³⁶ Becca, F., Tarquini, M., Grilli, M. & Di Castro, C. Charge-density waves and superconductivity as an alternative to phase separation in the infinite- U Hubbard-Holstein model. *Phys. Rev. B* **54**, 12443–12457 (1996). URL <https://link.aps.org/doi/10.1103/PhysRevB.54.12443>.
- ³⁷ Foussats, A. & Greco, A. Large- N expansion based on the Hubbard operator path integral representation and its application to the t – J model. II. The case for finite J . *Phys. Rev. B* **70**, 205123 (2004). URL <https://link.aps.org/doi/10.1103/PhysRevB.70.205123>.
- ³⁸ Bejas, M., Greco, A. & Yamase, H. Possible charge instabilities in two-dimensional doped mott insulators. *Phys. Rev. B* **86**, 224509 (2012). URL <https://link.aps.org/doi/10.1103/PhysRevB.86.224509>.
- ³⁹ Hybertsen, M. S., Stechel, E. B., Schluter, M. & Jennison, D. R. Renormalization from density-functional theory to strong-coupling models for electronic states in Cu-O materials. *Phys. Rev. B* **41**, 11068–11072 (1990). URL <https://link.aps.org/doi/10.1103/PhysRevB.41.11068>.
- ⁴⁰ Horio, M. *et al.* Three-dimensional fermi surface of overdoped la-based cuprates. *Phys. Rev. Lett.* **121**, 077004 (2018). URL <https://link.aps.org/doi/10.1103/PhysRevLett.121.077004>.

Supplemental Material:

Origin of the high-energy charge excitations observed by resonant inelastic x-ray scattering in cuprate superconductors

Andrés Greco[†], Hiroyuki Yamase^{*‡}, and Matías Bejas[†]

[†]*Facultad de Ciencias Exactas, Ingeniería y Agrimensura and Instituto de Física Rosario (UNR-CONICET), Av. Pellegrini 250, 2000 Rosario, Argentina*

[‡]*National Institute for Materials Science, Tsukuba 305-0047, Japan*

In this supplemental material we present i) essential part of our formalism, ii) analysis of individual charge excitations, and iii) short-range Coulomb interaction.

I. THEORETICAL SCHEME

In the path integral formalism¹, the Hamiltonian (1) can be written in terms of an effective model where fermionic fields interact with the six-component bosonic field

$$\delta X_i^a = (\delta R_i, \delta \lambda_i, r_i^x, r_i^y, A_i^x, A_i^y). \quad (4)$$

Here δR_i describes on-site charge fluctuations and is related to $X_i^{00} = N \frac{x}{2} (1 + \delta R_i)$ where X_i^{00} is the Hubbard operator² associated with the number of holes at a site i ; x is the doped carrier density per site; the factor N comes from the sum over the N fermionic channels after the extension of the spin index σ from 2 to N . $\delta \lambda_i$ describes fluctuations of the Lagrangian multiplier introduced to impose the constraint of non-double occupancy at any site. r_i^x and r_i^y (A_i^x and A_i^y) are fluctuations of the real (imaginary) part of a bond field along the x and y direction, respectively. These bond fields are Hubbard-Stratonovich fields, $\Delta_i^{x(y)}$, introduced to decouple the exchange interaction in the model (1) and are parametrized as $\Delta_i^{x(y)} = \Delta (1 + r_i^{x(y)} + i A_i^{x(y)})$, where Δ is the mean-field value of the bond field and is proportional to J . The bare propagator $D_{ab}^{(0)}(\mathbf{q}, i\omega_n)$ of the bosonic field δX^a is given by

$$[D_{ab}^{(0)}(\mathbf{q}, i\omega_n)]^{-1} = N \begin{pmatrix} \frac{x^2}{2} [V(\mathbf{q}) - J(\mathbf{q})] & \frac{x}{2} & 0 & 0 & 0 & 0 \\ \frac{x}{2} & 0 & 0 & 0 & 0 & 0 \\ 0 & 0 & \frac{4\Delta^2}{J} & 0 & 0 & 0 \\ 0 & 0 & 0 & \frac{4\Delta^2}{J} & 0 & 0 \\ 0 & 0 & 0 & 0 & \frac{4\Delta^2}{J} & 0 \\ 0 & 0 & 0 & 0 & 0 & \frac{4\Delta^2}{J} \end{pmatrix}, \quad (5)$$

where $J(\mathbf{q}) = \frac{J}{2}(\cos q_x + \cos q_y)$ and the matrix indices a and b run from 1 to 6; \mathbf{q} is a three dimensional wavevector and ω_n is a bosonic Matsubara frequency.

At leading order, the bare bosonic propagator is renormalized to be

$$D_{ab}^{-1}(\mathbf{q}, i\omega_n) = [D_{ab}^{(0)}(\mathbf{q}, i\omega_n)]^{-1} - \Pi_{ab}(\mathbf{q}, i\omega_n), \quad (6)$$

where $\Pi_{ab}(\mathbf{q}, i\omega_n)$ is the 6×6 bosonic self-energy

$$\begin{aligned} \Pi_{ab}(\mathbf{q}, i\omega_n) = & -\frac{N}{N_s N_z} \sum_{\mathbf{k}} h_a(\mathbf{k}, \mathbf{q}, \varepsilon_{\mathbf{k}} - \varepsilon_{\mathbf{k}-\mathbf{q}}) \frac{n_F(\varepsilon_{\mathbf{k}-\mathbf{q}}) - n_F(\varepsilon_{\mathbf{k}})}{i\omega_n - \varepsilon_{\mathbf{k}} + \varepsilon_{\mathbf{k}-\mathbf{q}}} h_b(\mathbf{k}, \mathbf{q}, \varepsilon_{\mathbf{k}} - \varepsilon_{\mathbf{k}-\mathbf{q}}) \\ & -\delta_{a1}\delta_{b1} \frac{N}{N_s N_z} \sum_{\mathbf{k}} \frac{\varepsilon_{\mathbf{k}} - \varepsilon_{\mathbf{k}-\mathbf{q}}}{2} n_F(\varepsilon_{\mathbf{k}}), \end{aligned} \quad (7)$$

due to the coupling between the bosonic field and fermionic fields; n_F is the Fermi-Dirac distribution function. The six components interaction vertex is given by

$$\begin{aligned} h_a(\mathbf{k}, \mathbf{q}, \nu) = & \left\{ \frac{2\varepsilon_{\mathbf{k}-\mathbf{q}} + \nu + 2\mu}{2} + 2\Delta \left[\cos\left(k_x - \frac{q_x}{2}\right) \cos\left(\frac{q_x}{2}\right) + \cos\left(k_y - \frac{q_y}{2}\right) \cos\left(\frac{q_y}{2}\right) \right]; 1; \right. \\ & \left. -2\Delta \cos\left(k_x - \frac{q_x}{2}\right); -2\Delta \cos\left(k_y - \frac{q_y}{2}\right); 2\Delta \sin\left(k_x - \frac{q_x}{2}\right); 2\Delta \sin\left(k_y - \frac{q_y}{2}\right) \right\}. \end{aligned} \quad (8)$$

The electronic dispersion $\varepsilon_{\mathbf{k}}$ is defined as

$$\varepsilon_{\mathbf{k}} = \varepsilon_{\mathbf{k}}^{\parallel} + \varepsilon_{\mathbf{k}}^{\perp}, \quad (9)$$

where the in-plane dispersion $\varepsilon_{\mathbf{k}}^{\parallel}$ and the out-of-plane dispersion $\varepsilon_{\mathbf{k}}^{\perp}$ are given, respectively, by

$$\varepsilon_{\mathbf{k}}^{\parallel} = -2 \left(t \frac{x}{2} + \Delta \right) (\cos k_x + \cos k_y) - 4t' \frac{x}{2} \cos k_x \cos k_y - \mu, \quad (10)$$

$$\varepsilon_{\mathbf{k}}^{\perp} = 2t_z \frac{x}{2} (\cos k_x - \cos k_y)^2 \cos k_z, \quad (11)$$

and μ is the chemical potential. Note that the bare hopping integrals t , t' , and t_z are renormalized by a factor $x/2$. No incoherent self-energy effects enter the fermionic dispersion at leading order. Note that k_z and q_z dependences enter only through $\epsilon_{\mathbf{k}-\mathbf{q}}$ in the first column in Eq. (8), whereas the other columns contain only the in-plane momentum \mathbf{q}_{\parallel} . In Eq. (7), N_s and N_z are the total number of lattice sites on the square lattice and the number of layers along the z direction, respectively.

All possible charge excitations in the layered t - J model are contained in $D_{ab}(\mathbf{q}, i\omega_n)$ [Eq. (6)] and can be treated on equal footing in the present theoretical scheme³. Usual charge fluctuations, namely $\chi_c(\mathbf{r}_i - \mathbf{r}_j, \tau) = \langle T_\tau n_i(\tau) n_j(0) \rangle$, are associated with the element $(1, 1)$ of the full 6×6 D_{ab} in Eq. (6) and is computed in \mathbf{q}_{\parallel} - ω space as^{3,4}

$$\chi_c(\mathbf{q}, i\omega_n) = -N \left(\frac{x}{2} \right)^2 D_{11}(\mathbf{q}, i\omega_n). \quad (12)$$

On the other hand, the elements from 3 to 6 of the matrix D_{ab} describe low-energy charge excitations associated with the charge order phenomenon³. Since we are interested in the high-energy charge excitations, we focus here on Eq. (12).

II. INDIVIDUAL CHARGE EXCITATIONS

The charge susceptibility $\chi_c(\mathbf{q}, i\omega_n)$ [Eq. (12)] contains both collective and individual excitations. It is not trivial to separate those excitations in a strong coupling model such as the t - J model. To extract the individual excitations, we consider a diagrammatic structure in the present large- N scheme and focus on contribution from a single bubble diagram. This single bubble is given by $\Pi_{22}(\mathbf{q}, i\omega_n)$. Intuitively this is clear because the vertex h_a of the single bubble should be constant for usual charge correlations, which is fulfilled only for the $a = 2$ component in Eq. (8). Mathematically we can show that the individual excitations are described by Π_{22} at leading order of the large- N scheme when we rewrite Eq. (12) in terms of Hubbard X -operators X_i^{p0} and X_i^{0p} by using the two constraints such as $X_i^{00} + \sum_p X_i^{pp} = \frac{N}{2}$ and $X_i^{pp'} = \frac{X_i^{p0} X_i^{0p'}}{X_i^{00}}$ (see Ref. 4). Therefore after the analytical continuation, we have computed $\text{Im}\Pi_{22}(\mathbf{q}, \omega)$ in Fig. 4. We have checked that the spectrum of $\text{Im}\Pi_{22}(\mathbf{q}, \omega)$ for a small Γ is indeed similar to the continuum spectrum of $\text{Im}\chi_c(\mathbf{q}, \omega)$ obtained in Fig. 2a, where the plasmon mode is well separated from the continuum spectrum.

III. SHORT-RANGE COULOMB INTERACTION

As a typical short-range Coulomb interaction, we may take

$$V(\mathbf{q}) = V_1(\cos q_x + \cos q_y) + V_2 \cos q_z . \quad (13)$$

The charge excitation spectrum for $V_2 = 0$ and $t_z = 0$ was already shown in Ref. 5, where a zero-sound mode is realized as collective excitations, which are gapless at $\mathbf{q}_{\parallel} = (0, 0)$; see Ref. 5 for more details of the zero-sound mode in the t - J model. In the present layered model with a finite t_z , however, the zero-sound mode acquires a gap at $\mathbf{q}_{\parallel} = (0, 0)$ for a finite q_z as shown in Fig. 5a. In Fig. 5 we have chosen $V_1 = V_2 = t$ after checking that qualitatively the same results are obtained for other choices of V_1 and V_2 as long as the system is stable in the presence of $V(\mathbf{q})$.

-
- ¹ A. Foussats and A. Greco, Phys. Rev. B **70**, 205123 (2004).
² J. Hubbard, Proc. R. Soc. London A **276**, 238 (1963).
³ M. Bejas, H. Yamase, and A. Greco, Phys. Rev. B **96**, 214513 (2017).
⁴ M. Bejas, A. Greco, and H. Yamase, Phys. Rev. B **86**, 224509 (2012).
⁵ A. Greco, H. Yamase, and M. Bejas, J. Phys. Soc. Jpn. **86**, 034706 (2017).